Thin films of hard cubic Zr_3N_4 stabilized by stress

MANISH CHHOWALLA* AND H. EMRAH UNALAN
Rutgers University, Ceramic and Materials Engineering, Piscataway, New Jersey 08854, USA
*e-mail: manish1@rci.rutgers.edu

Published online: 13 March 2005; doi:10.1038/nmat1338

Hard, refractory thin films consisting of group IVB element mono-nitrides deposited using various chemical and physical vapour-deposition techniques are widely used in wear-resistant applications. As the demand for performance exceeds the capabilities of existing materials, new materials with superior properties must be developed. Here we report the realization and characterization of hard cubic Zr_3N_4 (c-Zr_3N_4) thin films. The films, deposited using a novel but industrially viable modified filtered cathodic arc (FCA) method, undergo a phase transformation from orthorhombic to cubic above a critical stress level of 9 GPa as determined by X-ray diffraction and Raman spectroscopy. The c-Zr_3N_4 films are significantly harder (~36 GPa) than both the orthorhombic Zr_3N_4 (o-Zr_3N_4) and ZrN films (~27 GPa). The ability to deposit this material directly onto components as a thin film will allow its use in wear- and oxidation-resistant applications.

In addition to wear applications, nitride thin films are also widely used as brass-coloured decorative layers. Plasma-deposited nitride thin films (specifically zirconium nitride, ZrN) with superior hardness and corrosion resistance offer an environmentally friendly alternative to wet plating where a large amount of hazardous waste is generated. Nitride thin films such as TiN, ZrN, CrN and (Ti, Al)N are widely deposited at low temperatures (<400 °C) on an industrial scale using magnetron sputtering or cathodic arc plasmas[1–3]. Mono-nitride thin films adopt the NaCl structure and are highly conductive owing to a finite density of states at the Fermi level from the residual electron contributed by each atom in the metal *d* band.

Although it is generally difficult to vary the concentration of nitrogen in nitride thin films, metastable higher nitrides with a composition of M_3N_4 (where M is either Hf or Zr) and orthorhombic structure have also been reported[4–11]. These nitrogen-rich films are transparent and much less conducting than the mono-nitrides. Bulk samples of higher-density cubic Zr_3N_4 and Hf_3N_4 (c-M_3N_4) with thorium phosphide (Th_3P_4) structure have been synthesized by Zerr *et al.* using a high-pressure laser-heated diamond anvil cell[12]. Their results showed that the c-Zr_3N_4 formed at a pressure of 15.6–18 GPa and temperature of 2,500–3,000 K whereas the c-Hf_3N_4 phase could be obtained at 18 GPa and 2,800 K. The transition metal M_3N_4 phases are similar to the group IVA element nitrides (M_3N_4 where M = Si, Ge, Sn), which also show low- and high-density phases[13–15]. The high-density γ phases of these nitrides with spinel structure, which are comparable to the c-M_3N_4 of transition metal nitrides, show extraordinary mechanical and electrical properties, which make them useful in many applications ranging from abrasives to material for blue LEDs. Following the experimental result of Zerr *et al.*[12], several theoretical studies[16–19] have been undertaken to understand and explore new properties of different phases of M_3N_4. The calculations indicate these new materials have extraordinary oxidation resistance and are expected to be nearly as hard as γ-Si_3N_4 and also semiconducting with a bandgap of around 1.5 eV. Indeed, Zerr *et al.* reported a high bulk modulus of 250 GPa for both c-Zr_3N_4 and c-Hf_3N_4 indicating high hardness and they also found that c-Hf_3N_4 was transparent[12].

In this work, we describe the deposition and characterization of cubic Zr_3N_4 thin films. These novel thin films were deposited using a novel modified filtered cathodic arc (FCA) where the metal vapour, generated by an arc discharge on pure zirconium cathode, was

© 2005 Nature Publishing Group

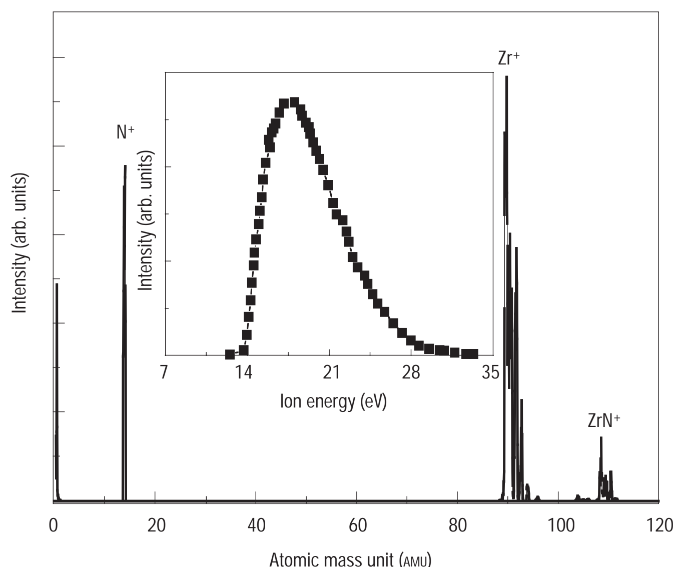

Figure 1 Mass spectrum and ion-energy distribution (inset) of Zr-N plasma produced by the modified filtered cathodic arc. Three distinct mass peaks attributed N^+, Zr^+ and ZrN^+ charge states can be clearly observed. The Zr^+ and ZrN^+ mass peaks can be deconvoluted in to three peaks associated with the most prevalent isotopes of Zr. The possibility of N_2^{++} peak contributing to the N^+ peak was eliminated by closely monitoring the peak at 14.5 AMU from the ^{15}N isotope. The absence of the 14.5 AMU peak indicates the peak at 14 AMU is entirely from N^+. Note that the intensity is in linear scale. The narrow ion-energy distribution of the Zr^+ species in the inset reveals a peak energy of ~18 eV. The N^+ and ZrN^+ species also exhibited similar energy distribution. The plasma characteristics were measured using a Hiden EQP Analyzer equipped with mass spectrometer located at the exit of magnetic filter ~50 cm from the Zr cathode.

Table 1 Comparison of c-Zr_3N_4 calculated and measured XRD peak positions as well as spacings measured by electron diffraction. The calculated Cu Kα XRD pattern was based on a cubic structure in a *I*-centred lattice space group (*I*43*d* with a lattice parameter 6.740 Å), as reported by Zerr *et. al.*[12] and others[16,19].

hkl	Theoretical *d* values	Theoretical 2*θ*	Measured 2*θ* (XRD)	Measured 2*θ* (ED)
211	2.75159	32.514	32.703	32.5
220	2.3895	37.720		
310	2.13138	42.374	41.260	42.4
321	1.80134	50.634	51.063	
400	1.68500	54.407		
420	1.50711	61.476	61.324	
332	1.43697	64.831		64.75
422	1.37580	68.097	68.962	
510 or 431	1.32182	71.289	71.29	
521	1.23055	77.508		
440	1.19147	80.558		
530	1.1559	83.581		
611 or 532	1.09337	89.581		

reacted with fully ionized atomic nitrogen. The plasma conditions generated by our modified FCA are unique and allow unprecedented control over the ion energy and flux. The zirconium nitride thin films deposited using our technique have Zr_3N_4 stoichiometry in contrast to films deposited by unmodified FCA, which are ZrN. The structure of our Zr_3N_4 films was determined by X-ray diffraction (XRD), electron diffraction in transmission electron microscope (TEM) and by Raman spectroscopy. Thin films were deposited at several ion energies with modified and unmodified FCA. Our results indicate that the cubic Zr_3N_4 is obtained at optimum ion energy ranging from 100–200 eV, which also correlated to the most highly stressed films. The compressive stress appears to be the key factor in obtaining the cubic versus the orthorhombic structure for Zr_3N_4. That is, films with Zr_3N_4 stoichiometry but with stress less than ~9 GPa have the orthorhombic crystal structure, whereas higher stress values yield the cubic structure. The hardness of the c-Zr_3N_4 films measured using nano-indentation was found to be substantially higher (~36 GPa) than for films with orthorhombic or NaCl structures (~27 GPa). The films were also transparent with an absorption edge at around 1.6 eV.

Cathodic arc is an important source of highly ionized and directed plasma beams for energetic deposition of thin films. The high level of ionization in the plasma allows for precise control of the ion energy by applying a bias to the substrates. The ability to control the ion energy allows tunability of the thin-film structure. A quarter torus magnetic solenoid is generally used to filter out microscopic particles (referred to as 'macro-particles') that are also generated during the arc discharge. Thus the filtered plasma at the exit of the plasma duct is essentially free of macro-particles, allowing the deposition of atomically smooth, high-quality thin films[20–22]. Although the metal vapour in FCA is completely ionized, the degree of ionization of the reaction gas (nitrogen in the case of nitrides) is relatively small (~10%). The lack of ionization leads to inefficient reactions and also broadens the ion-energy distribution of the impinging flux.

We have used a modified FCA process, which leads to a fully ionized plasma consisting of singly charged Zr^+, N^+ and ZrN^+ species to obtain the c-Zr_3N_4 phase. The modified method is similar to the unmodified FCA in all respects except that the nitrogen gas inlet into the chamber is by a 1-mm hole in the Zr cathode on which the arc discharge occurs[23–26]. This is similar to our previously reported localized high-pressure arc discharge (LHPAD) used to deposit ultra-hard and elastic carbon thin films[27] and low friction MoS_2 thin films[28]. In LHPAD, the high pressure above the arc spot is used to quench the vapour and form nanoparticles, which are then condensed onto a substrate. In the experiments reported here, we introduce the reactive gas at the arc spot in order to enhance the formation of zirconium nitride on the cathode surface (referred to as poisoning). By adjusting the flow rate and pressure of the gas, it is possible to consume all of the nitrogen in the poisoning reaction[29]. The poisoning of the cathode surface means that the arc effectively runs on a nitride surface rather than pure Zr metal. The degree of poisoning is significantly enhanced in our modified FCA and thus our plasma characteristics show only singly charged Zr^+,

© 2005 Nature Publishing Group

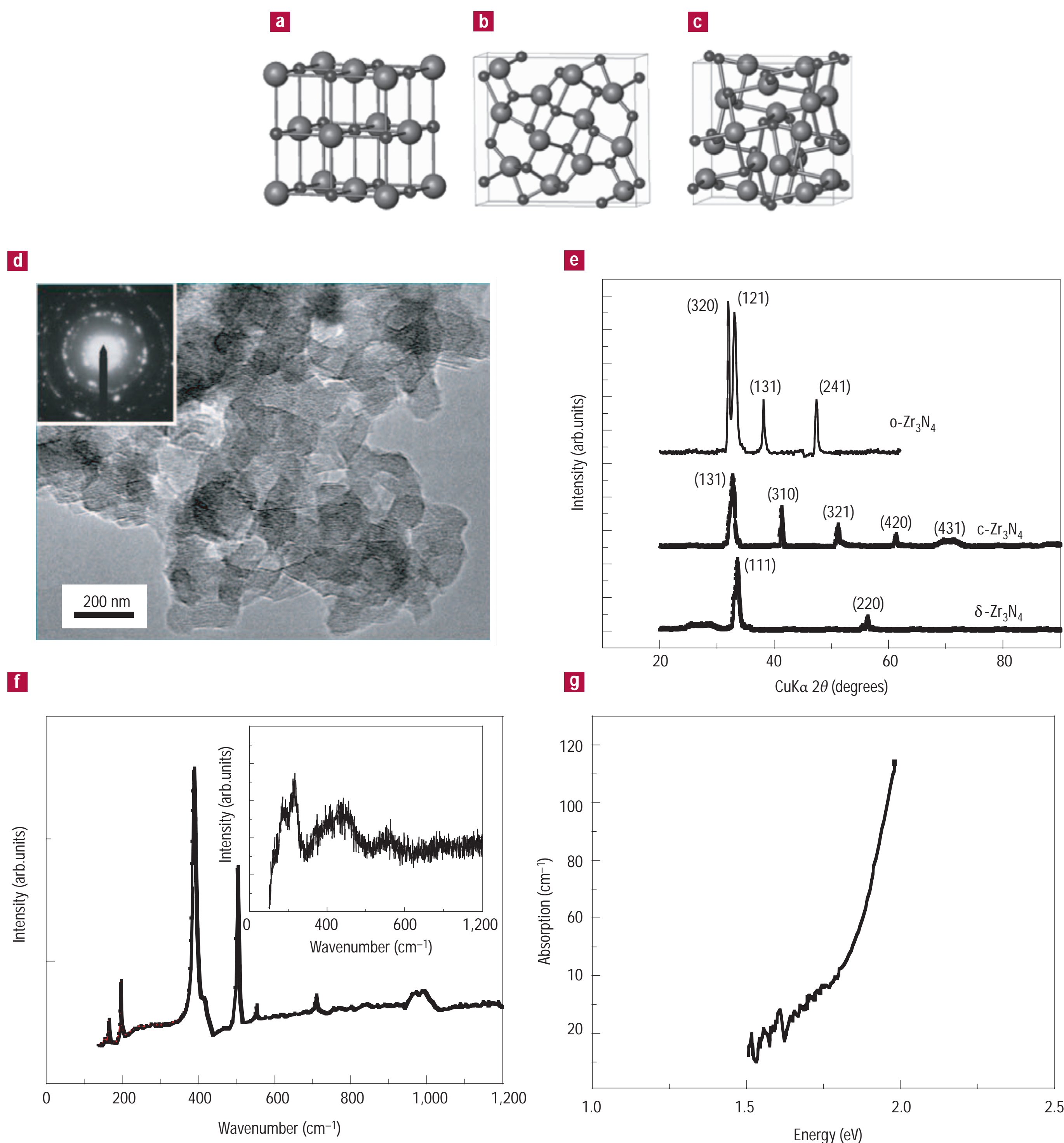

Figure 2 Crystal structures, XRD, TEM, Raman and UV-VIS spectroscopy data for various Zr-N thin films investigated in this study. Crystal structure of **a**, ZrN based on the rock salt NaCl structure; **b**, orthorhombic Zr_3N_4 based on the space group *Pnam*; and **c**, the cubic Zr_3N_4 structure based on the $I\bar{4}3d$ space group. **d**, TEM image of 100-nm c-Zr_3N_4 thin films deposited on salt. The TEM samples were produced by dissolving the salt in de-ionized water. The images were obtained using a JEOL 2000FX TEM operated at 200 kV. The inset shows the electron diffraction pattern used to calculate the 2θ values in Table 1. **e**, XRD patterns from three types of Zr-N films produced by the filtered cathodic arc. The XRD was performed, using a Siemens MRD diffractometer with a Cu source, on 0.75-µm thin films deposited on Si substrates. In order to enhance the signal from the thin films, all measurements were performed at low grazing angles. The Si peaks from the XRD spectra have been removed for clarity. **f**, Raman spectrum of c-Zr_3N_4 thin films measured using a Renishaw Raman microscope with 514.5 nm Ar laser. The inset shows the Raman spectrum for ZrN films. **g**, Typical optical absorption properties of c-Zr_3N_4 deposited on quartz substrates. The absorption was measured using an UV-VIS spectrometer (Phillips two beam) with wavelengths in the 200 to 900 nm range.

© 2005 Nature Publishing Group

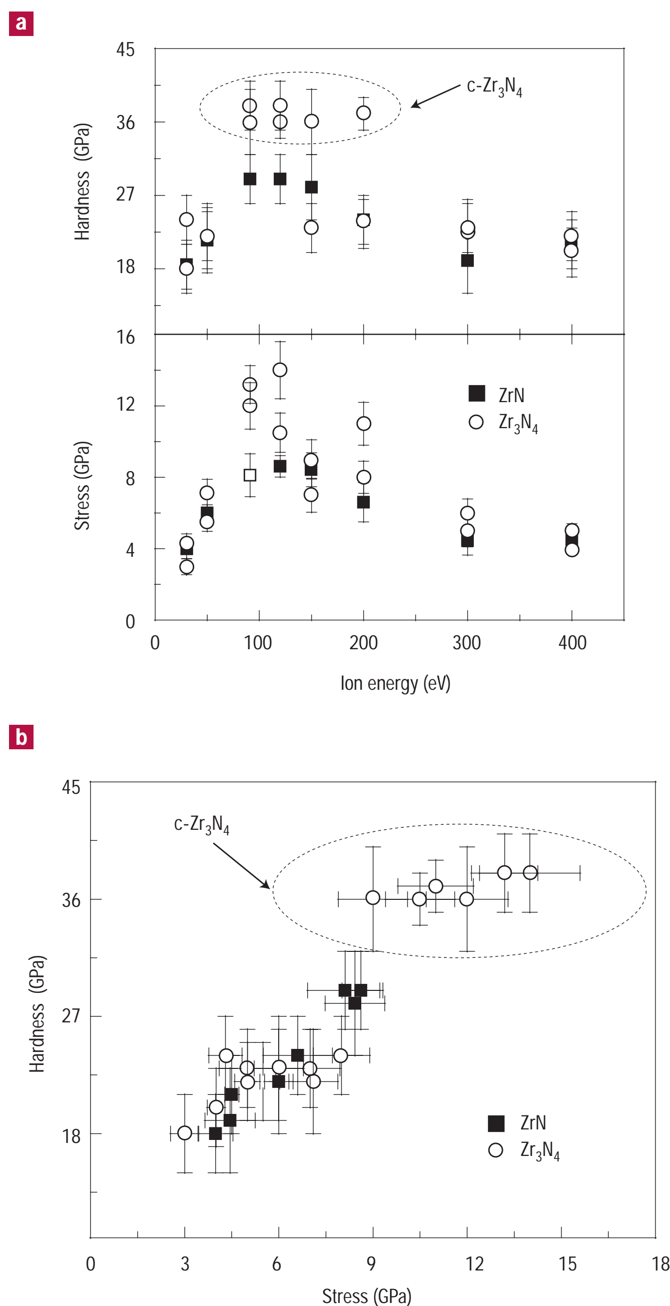

Figure 3 Variation of hardness and stress versus ion energy and the dependence of hardness on the stress. Film thickness was 780 nm. **a**, Hardness and compressive stress versus ion energy for Zr-N films deposited using the unmodified and modified filtered cathodic arc. Both properties show similar trends with ion energy, peaking at 100 to 200 eV. Films with the highest hardness were found to be c-Zr_3N_4, as indicated. The hardness was measured using a Nanoindenter II nanoindentation machine with a Berkovich tip. The maximum applied load was 5 mN, which yielded a maximum displacement of around 80 nm. The compressive stress in the films was obtained from the curvature of the Si substrate before and after the film deposition[27,29]. **b**, Cubic Zr_3N_4 hardness versus the compressive stress. Films with the highest stress were found to be c-Zr_3N_4, whereas the low-stress films deposited by the modified FCA had the orthorhombic structure. The error bars represent the standard deviation of at least five measurements.

Table 2 Comparison of Raman peak positions (cm^{-1}) of our c-Zr_3N_4 thin films and bulk samples fabricated by Zerr *et al.*[12]. Calculated values reported by Kroll *et al.*[16] are also shown.

Bulk c-Zr_3N_4	Thin film c-Zr_3N_4	Calculated values
163	165	165
196	195	282
387	387	368
416	415	423
551	550	506
707	710	670

N^+ and ZrN^+ species (Fig. 1) as expected from an arc discharge on Zr-N. That is, the arc evaporates Zr-N and then through collisions the compound is ionized or dissociated into Zr and N, which can be ionized through additional collisions. The narrow ion-energy distribution of the plasma is shown in the inset of Fig. 1. The fully ionized plasma with a narrow ion-energy distribution function provide significantly better control over the deposition parameters than previously reported of Zr-N plasmas[29], which we believe is essential for creating conditions for the formation of the metastable c-Zr_3N_4 phase.

The stoichiometry of all films deposited using the modified FCA was measured by Rutherford backscattering and found to be Zr_3N_4, whereas the unmodified FCA yielded only the mono-nitride. The oxygen content in the film was negligible. The three zirconium nitride crystal structures (rock salt, orthorhombic Zr_3N_4 (o–Zr_3N_4) and cubic Zr_3N_4) encountered in this study are shown in Fig. 2a–c. The TEM image of our polycrystalline films with crystallite sizes ranging from 100 – 200 nm is shown in Fig. 2d. The electron diffraction pattern is shown in the inset of the image and the spacings measured from the pattern are listed in Table 1. XRD spectra of Zr_3N_4 and ZrN films are shown in Fig. 2e. In the case of Zr_3N_4, two distinct XRD spectra, characteristic of orthorhombic and cubic crystal structures, were obtained, whereas the ZrN films exhibited the typical NaCl cubic structure (referred to as δ-ZrN). The comparison of the measured and calculated XRD peak positions of the c-Zr_3N_4 phase are given in Table 1. The XRD spectra and peak positions of the orthorhombic Zr_3N_4 and ZrN films match well with other reports in the literature[10,30]. Although no experimental XRD spectrum for c-Zr_3N_4 is available for comparison, we have calculated the XRD spectrum based on the experimental data of Zerr *et al.*[12] and theoretical calculations by others[16,19]. It can be seen from Table 1 that our measured electron-diffraction spacings and XRD peak positions for c-Zr_3N_4 films match well with the calculated values, indicating that we have been successful in depositing the phase as a thin film. The slight deviations between the experimental and calculated lattice parameters in Table 1 are attributed to displacement of atoms due to ion bombardment during growth. That is, the creation of vacancies and interstitials during energetic condensation of the impinging ions is probably responsible for the variation in atomic positions in the lattice of our c-Zr_3N_4 thin films.

In addition to the diffraction data, we have also confirmed the deposition of the c-Zr_3N_4 phase through Raman spectroscopy. The Th_3P_4 structure of Zr_3N_4 contains 14 atoms in its unit cell and has T_d point group. The group theory analysis yields the following

© 2005 Nature Publishing Group

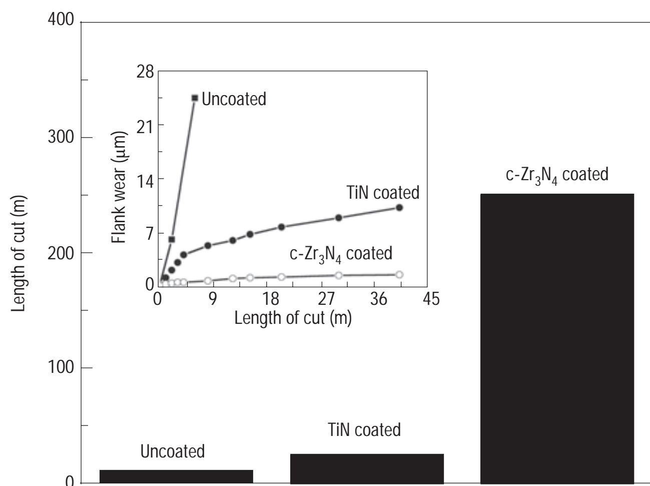

Figure 4 Milling test results from uncoated, TiN and c-Zr_3N_4-coated three flute end mills with a diameter of 8 mm. The milled material was AISI 1045 steel. The rotation speed of was 200 m min^{-1} and the feed rate was 10 m min^{-1}. The depth of cut was approximately 1.5–2.0 mm. Standard coolant was used during machining. The cutting was stopped after 250 m. The film thickness for both FCA TiN and c-Zr_3N_4 was kept constant at 1.2 µm. Uniform coating on the end mill was achieved by rotating the end mills during deposition. The inset shows the wear after milling various lengths of the low carbon steel.

vibrational modes: $\Gamma^{\rm opt} = A_1 + 2A_2 + 3E + 5T_1 + 5T_2$ where A_1, E and T_2 modes are Raman active[16]. The Raman spectrum of our c-Z_3N_4 thin films is shown in Fig. 2f. The Raman analysis revealed six vibrational modes, which are in excellent agreement with the results of Zerr *et al.*[12]. A strong peak ~387 cm^{-1} with a shoulder at around ~415 cm^{-1} is clearly visible along with less intense peaks at ~165 cm^{-1}, ~195 cm^{-1}, ~550 cm^{-1} and ~710 cm^{-1}. In addition to these peaks, there are also two peaks (~500 cm^{-1} and 980 cm^{-1}) that correspond to the silicon substrates on which the films are deposited and thus indicate that the c-Zr_3N_4 phase is transparent. This is in agreement with our optical measurements of the films, which show an absorption edge at ~1.6 eV (Fig. 2g). In the inset of Fig. 2f, we have also included the Raman spectrum of δ-ZrN, which shows typical features[31]. Comparison of phonon modes from our c-Zr_3N_4 thin films and from bulk samples of Zerr *et al.*[12] along with calculated values[16] are listed in Table 2. It can be seen that the two experimental values are in very good agreement but differ slightly from the calculated values. Thus our Raman data is consistent with the diffraction data and indicate that we have been successful in depositing the cubic phase of Zr_3N_4.

The FCA has been used previously to obtain the metastable highly tetrahedral amorphous carbon phase through deposition at optimum ion energy and temperature[32,33]. We have carried out a similar experiment to investigate whether a phase change in zirconium nitride can be induced through adjusting the plasma parameters. The variation of hardness and compressive stress as a function of the ion energy are shown in Fig. 3a. The optimum ion energy for achieving the maximum hardness of these films is between 100 to 200 eV. The highest hardness values are also correlated to the highest stress values. The linear correlation between the hardness and stress is illustrated in Fig. 3b. It can be seen in Fig. 3a that the ZrN films follow a similar trend to the Zr_3N_4 films and do not undergo any dramatic changes in structure or stoichiometry. In contrast, we have found that the Zr_3N_4 thin films undergo orthorhombic to cubic phase change at ion energies ranging from 100 to 200 eV. Our data shown in Fig. 3a and b show that the films with the highest stress and highest hardness are of the cubic phase. Furthermore, we find that films with a stress value above ~9 GPa have cubic structure, whereas films with stress values less than ~9 GPa, even those deposited between 100 to 200 eV, have the orthorhombic crystal structure. Therefore, the compressive stress in the films (and not the ion energy) appears to be the key factor in nucleating the metastable cubic phase. Currently we are investigating why few films deposited at the optimum ion energy of 100 to 200 eV have low stress and thus are orthorhombic whereas most films are cubic. We also argue that the significantly higher hardness values of the denser c-Zr_3N_4 phase are intrinsic of the material and not entirely stress induced.

We now discuss the possible mechanism for the formation of the metastable c-Zr_3N_4 phase. Stress-induced stabilization of a metastable phase has been widely demonstrated in many materials[32,34]. Furthermore, although the overall stress in a thin film can be low, high stress regions may lead to nucleation of a metastable phase. Mckenzie has shown that the hydrostatic stress in a thin film is approximately equivalent to two thirds of the biaxial stress when the shear stress is ignored[32,34]. Stress relaxation in thin films can take place through shearing of the material or the substrate. Therefore, harder materials can withstand much higher compressive stresses due to the superior shear strength. This is the case in Fig. 3b where the harder c-Zr_3N_4 thin films have significantly larger stress. As the threshold stress for phase transformation is approximately 9 GPa, the hydrostatic stress experienced by the film is ~6 GPa. Although this value is lower than the ~15 GPa reported by Zerr *et al.*[12], recent calculations[35] indicate that a pressure of only 6 GPa is sufficient for stabilization of the metastable c-Zr_3N_4 phase. The bulk temperature of the substrate during deposition was held at 400 °C although the actual temperature near the growth zone will be significantly higher due to ion-energy dissipation. It is difficult to estimate the temperature in the growth zone but calculations based on the thermal spike model indicate temperatures can be as high as 3,000 K (ref. 36). Thus the high temperature and hydrostatic stress conditions created by adjusting the deposition conditions are thermodynamically similar to those reported by Zerr *et al.*[12], and thus favourable for the formation of the metastable c-Zr_3N_4 thin films.

In order to translate the extraordinary properties of the cubic phase into real applications, we have coated carbide end mills with the c-Zr_3N_4 coating and performed milling tests. The results of the tests are shown in Fig. 4. It can be clearly seen that the c-Zr_3N_4 coating dramatically outperforms the uncoated tool as well the end mill coated with the traditional TiN. Furthermore, the actual wear on the flank of the end mill is shown in the inset of Fig. 4. The flank wear was also found to be dramatically better than the uncoated as well the TiN coated tool. These results indicate that the c-Zr_3N_4 phase has great potential as a wear-resistant layer.

Our findings indicate that the metastable phase is stabilized by the large stress and high temperature in the growth zone, which create suitable thermodynamic conditions for stabilization of the cubic phase. It may also be possible to deposit other nitrides such as γ-Si_3N_4 and Ge_3N_4 as thin films using our technique. Finally, in contrast to bulk synthesis, the ability to deposit this hard nitride phase as a thin film will allow its widespread use as oxidation- and wear-resistant layers on automotive parts and tool components.

METHODS

The Zr-N thin films were deposited using filtered cathodic arc apparatus (duct diameter = 12 cm). The base pressure achieved before all depositions was 2×10^{-7} torr. The magnetic field used to guide the plasma around the 90° bend was 30 mTesla. A high purity (99.6%), cylindrical cathode (diameter = 6.25 cm, height = 5 cm) was used as the plasma source. The cathode was powered by a direct current arc welding power supply. The arc was ignited by touching an earthed anode (Mo rod with a diameter of 3 mm) to the cathode. The nitrogen in the unmodified FCA depositions was introduced near the cathode. In the modified FCA case, the nitrogen was introduced through a

© 2005 Nature Publishing Group

1 mm hole in the Zr cathode. The complete poisoning of the cathode surface was found to occur at a pressure of 4×10^{-4} torr. At this pressure, virtually all the nitrogen is consumed by the cathode so that no molecular nitrogen could be detected by our Hiden EQP plasma analyser. In this study, all depositions were carried out at an arc current of 75 A and voltage of 19 V. The ion flux at the cathode was kept constant at 4.7 mA cm^{-2} to obtain a deposition rate of ~2 nm s^{-1}. The substrate temperature was adjusted to 400 °C before deposition using a resistive heater and monitored by a thermocouple. The ion energy was controlled by applying a bias voltage using an Advanced Energy 1kW MDX generator. The approximate total ion energy was obtained by adding the initial energy of the ions plus the applied bias. The thicker films were deposited using the two-step process[37] where the first step is the creation of an interface layer through ion bombardment at ~1,000 eV (current density = 4.5 mA cm^{-2} for 30 seconds). Subsequent to the ion bombardment, the bias voltage was reduced to –100 V to deposit the c-Zr_3N_4 phase. The creation of the interfacial layer through the initial high-energy bombardment seems to provide suitable adhesion of the highly stressed films to the substrate, although direct measurement of the adhesion is still underway.

Received 2 October 2004; accepted 17 January 2005; published 13 March 2005.

References

1. Johansson, B. O., Sundgren, J. E., Greene, J. E., Rockett, A. & Barnett, S. A. Growth and properties of single crystal TiN films deposited by reactive magnetron sputtering. *J. Vac. Sci. Technol. A* **3,** 303–307 (1985).
2. Martin, P. J. *et al.* Characteristics of titanium arc evaporation processes. *Thin Solid Films* **153,** 91–102 (1987).
3. Sanders, D. M., Boercker, D. B. & Falabella, S. Coating technology based on the vacuum arc – a review. *IEEE T. Plasma Sci.* **18,** 883–894 (1990).
4. Schwarz, K., Williams, R. A., Cuomo, J. J., Harper, J. H. E. & Hentzell, H. T .G. Zirconium nitride – a new material for Josephson junctions. *Phys. Rev. B* **32,** 8312–8316 (1985).
5. Johansson, B. O., Hentzell, H. T. G., Harper, J. M. E. & Cuomo, J. J. Higher nitrides of hafnium, zirconium and titanium synthesized by dual ion beam deposition. *J. Mater. Res.* **1,** 442–451 (1986).
6. Salmenoja, K., Korhonen, A. S., Erola, E. & Molarius, J. M. Stability of nitrogen rich titanium nitride and zirconium nitride films. *Appl. Phys. Lett.* **49,** 505–506 (1986).
7. Prieto, P., Galan, L. & Sanz, J. M. Electronic structure of insulating zirconium nitride. *Phys. Rev. B* **47,** 1613–1615 (1993).
8. Prieto, P. *et al.* Electronic structure of insulating Zr_3N_4 studied by resonant photoemission. *Phys. Rev. B* **51,** 17984–17986 (1995).
9. Lerch, M., Fuglein, E. & Wrba, J. Synthesis, crystal structure and high temperature behavior of Zr_3N_4. *Z. Anorg. Allg. Chem.* **622,** 367–372 (1996).
10. Wang, L., Yin, M. & Zhu, Y. Study of interface diffusion between Zr_3N_4 and stainless steel. *Surf. Interface Anal.* **35,** 814–817 (2003).
11. Becker, J. S., Kim, E. & Gordon, R. G. Atomic layer deposition of insulating hafnium and zirconium nitrides. *Chem. Mater.* **16,** 349–3501 (2004).
12. Zerr, A., Miehe, G. & Riedel, R. Synthesis of cubic zirconium and hafnium nitride having Th_3P_4 structure. *Nature Mater.* **2,** 185–189 (2003).
13. Zerr, A. *et al.* Synthesis of cubic silicone nitride. *Nature* **400,** 340–342 (1999).
14. Sekine, T., Hongliang, H., Kobayashi, T., Zhang, M. & Fangfang, X. Shock induced transformation of β-Si_3N_4 to a high pressure cubic-spinel phase. *Appl. Phys. Lett.* **76,** 370–3708 (2000).
15. Leinenweber, K. *et al.* Synthesis and structure refinement of the spinel γ-Ge_3N_4. *Chem. Eur. J.* **5,** 3076–3078 (1999).
16. Kroll, P. Hafnium nitride with thorium phosphide structure: physical properties and an assessment of the Hf-N, Zr-N, and Ti-N phase diagrams at high pressures and temperatures. *Phys. Rev. Lett.* **90,** 125501 (2003).
17. Dong, J. J., Deslippe, J., Sankey, O. F., Soignard, E. & McMillan, P. F. Theoretical study of the ternary spinel nitride system Si_3N_4-Ge_3N_4. *Phys. Rev. B* **67,** 094104 (2003).
18. Ching, W.-Y., Xu, Y. N. & Ouyang, L. Electronic and dielectric properties of insulating Zr_3N_4. *Phys. Rev. B* **66,** 235106 (2002).
19. Mattesini, M., Ahuja, R. & Johansson, B. Cubic Hf_3N_4 and Zr_3N_4: a class of hard materials. *Phys. Rev. B* **68,** 184108 (2003).
20. Aksenov, I. I. *et al.* Influence of electron magnetization of vacuum arc plasma on reaction kinetics in the synthesis of nitride containing coatings. *Zh. Tekh. Fiz.* **51,** 303–309 (1981).
21. Anders, A. Approaches to rid cathodic arc plasmas of macro- and nanoparticles: a review. *Surf. Coat. Technol.* **121,** 319–330 (1999).
22. Martin, P. J. & Bendavid, A. Review of the filtered vacuum arc process and materials deposition. *Thin Solid Films* **391,** 1–15 (2001).
23. Rogozin, A. F. & Fontana, R. P. Reactive gas-controlled arc process. *IEEE Trans. Plasma Sci.* **25,** 680–684 (1997).
24. Boxman, R. L., Goldsmith, S., Brosh, N., Shalev, S. & Yaloz, H. Method and apparatus for surface-treating workpieces. US Patent 4,645,895 (1987).
25. Demidenko, I. I., Lomino, N. S., Ovcharenko, V. D., Padalka, V. G. & Polyakova, G. N. Ionization mechanism of reaction gas in vacuum-arc discharges. **54,** *Zh. Tekh. Fiz.* 1534–1537 (1984).
26. Aksenov, I. I. *et al.* Influence of electron magnetization of vacuum-arc plasma on reaction kinetics in the synthesis of nitride containing coats. **17,** *Zh. Tekh. Fiz.* 200–202 (1983).
27. Amaratunga, G .A. J. *et al.* Hard elastic carbon thin films from linking of carbon nanoparticles. *Nature* **383,** 321–323 (1996).
28. Chhowalla, M. & Amaratunga, G. A. J. Thin films of fullerene-like MoS_2 nanoparticles with ultra-low friction and wear. *Nature* **407,** 164–167 (2000).
29. Chhowalla, M. Ion energy and charge state distributions in zirconium nitride arc plasma. *Appl. Phys. Lett.* **83,** 1542–1544 (2003).
30. Wu, D., Zhang, Z., Fu, W., Fan, X. & Guo, H. Structure, electrical and chemical properties of zirconium nitride films deposited by dc reactive magnetron sputtering. *Appl. Phys. A* **64,** 593–598 (1997).
31. Chen, X. J. *et al.* Pressure-induced phonon frequency shifts in transition-metal nitrides. *Phys. Rev. B* **70,** 014501 (2004).
32. McKenzie, D. R., Muller, D. & Pailthorpe, B. A. Compressive stress induced formation of thin film tetrahedral amorphous carbon, *Phys. Rev. Lett.* **67,** 773–776 (1991).
33. Chhowalla, M. *et al.* Influence of ion energy and substrate temperature on the optical and electronic properties of tetrahedral amorphous carbon (ta-C) films. *J. Appl. Phys.* **81,** 139–145 (1997).
34. McKenzie, D. R. Generation and applications of compressive stress induced by low energy ion bombardment. *J. Vac. Sci. Technol. B* **11,** 1928–1935 (1993).
35. Kroll, P. Assessment of the Hf-N, Zr-N and Ti-N phase diagrams at high pressures and temperatures: balancing between MN and M_3N_4 (M = Hf, Zr, Ti). *J. Phys. Condens. Matter* **16,** S1235–S1244 (2004).
36. Robertson, J. Deposition mechanisms for promoting sp^3 bonding in diamond-like carbon. *Diam. Relat. Mater.* **2,** 984–989 (1993).
37. Chhowalla, M. Thick, well-adhered, highly stressed tetrahedral amorphous carbon. *Diam. Relat. Mater.* **10,** 1011–1016 (2001).

Acknowledgements

The authors would like to thank Rob Aharonov of Ion Bond (Madison Height, Michigan) for providing the modified FCA cathode assembly as well as advice and support for the project.
Correspondence and requests for materials should be addressed to M.C.

COMPETING FINANCIAL INTERESTS

The authors declare that they have no competing financial interests.

© 2005 Nature Publishing Group